The Oxo-bridge Scenario Behind Single Site Water Oxidation Catalysts

Isidoro López,[a] Somnath Maji,[a] J. Benet-Buchholz[a] and Antoni Llobet[a,b,]*

[a]Institute of Chemical Research of Catalonia (ICIQ), Av. Països Catalans, 16, 43007 Tarragona, Spain.

[b]Departament de Química, Universitat Autònoma de Barcelona, Cerdanyola del Vallès, 08193 Barcelona, Spain.

KEYWORDS. Water oxidation, redox catalysis, Ru-oxo bridged complexes, transition metal complexes.

ABSTRACT. High oxidation state decay of mononuclear complexes $[RuTB(H_2O)]^{2+}$, $\mathbf{X}^{2+}$, (where B = 2,2'-bpy or bpy for X = 1; B = 5,5'-F_2-bpy for X = 2; B = 6,6'-F_2-bpy for X = 3; T = 2,2':6',2''-terpyridine) oxidized with a large excess of Ce(IV) generates a manifold of polynuclear oxo-bridged complexes. This include: a) dinuclear, $[TB\text{-}Ru^{IV}\text{-}O\text{-}Ru^{IV}\text{-}(T)(O)OH_2]^{2+}$ (**1-dn**$^{4+}$), $[TB\text{-}Ru^{III}\text{-}O\text{-}Ru^{III}\text{-}T(MeCN)_2]^{4+}$ (**1-dn-N**$^{4+}$), $\{[Ru^{III}(trpy)(bpy)]_2(\mu\text{-}O)\}^{4+}$, (**1-dm**$^{4+}$**)**; b) trinuclear $\{[Ru^{III}(trpy)(bpy)(\mu\text{-}O)]_2Ru^{IV}(trpy)(H_2O)\}(ClO_4)_5^{6+}$ (**1-tr**$^{6+}$), $\{[Ru^{III}(trpy)(bpy)(\mu\text{-}O)]_2Ru^{IV}(pic)_2\}(ClO_4)_4$ (**1-tr-P**$^{4+}$; where P is the 2-pyridine carboxylate anion); and c) tetranuclear, $[TB\text{-}Ru^{III}\text{-}O\text{-}TRu^{IV}(H_2O)\text{-}O\text{-}TRu^{IV}(H_2O)\text{-}O\text{-}Ru^{III}\text{-}TB]^{8+}$ (**1-tn**$^{8+}$), $[TB\text{-}Ru^{III}\text{-}O\text{-}TRu^{IV}(AcO)\text{-}O\text{-}TRu^{IV}(AcO)\text{-}O\text{-}Ru^{III}\text{-}TB]^{6+}$ (**1-tn-Ac**$^{6+}$) and $[TB\text{-}Ru^{II}\text{-}O\text{-}TRu^{IV}(MeCN)\text{-}O\text{-}TRu^{IV}(MeCN)\text{-}O\text{-}Ru^{II}\text{-}TB]^{6+}$ (**1-tn-N**$^{6+}$) complexes. These complexes have been structurally characterized by single crystal X-ray diffraction analysis and their structural properties correlated with their electronic structure. The dinuclear **1-dm**$^{4+}$ complex has been further characterized by spectroscopic and electrochemical techniques. Addition of excess Ce(IV) to **1-dm**$^{4+}$ generates dioxygen in a catalytic manner. However resonance Raman spectroscopy points out to the *in situ* formation of **1-dn**$^{4+}$ as the active species.

1. Introduction.

The oxo-bridge metal unit is a ubiquitous motif in bioinorganic chemistry. There is a large number of metalloproteins[1-3] that contain the Fe-O-Fe core whereas the oxygen evolving complex (OEC) of photosystem II (PSII) contains Mn-O-Mn units, within its CaMn4 cluster. The latter has gained an increasing attention because it performs the key reaction that needs to be fully understood and mastered to be able to come up with the development of commercial devices, for the efficient conversion of sunlight into chemical fuels such as H_2 or CH_3OH.

To mimic the functional properties of OEC, many polynuclear μ-oxo metal complexes with high oxidation states have been synthesized. The blue dimer was the first reported molecularly well characterized water oxidation catalyst (WOC) and contains a Ru^{III}-O-Ru^{III} unit. Other polynuclear WO catalysts recently reported include complexes with rigid aromatic organic bridging ligands instead of the oxo-bridge[4-8] as well as a family of polyoxometalate complexes.[9-12]

On the other hand, the recent discovery of single site WOCs[5, 13, 14] has generated a large body of complexes that are proposed to remain as mononuclear species during the catalytic cycle. The successive pathways that lead to the evolution of dioxygen in complexes related to $[RuTB(H_2O)]^{2+}$, $\mathbf{X}^{2+}$, (where B = 2,2'-bpy or bpy for X = 1; B = 5,5'-F_2-bpy for X = 2; B = 6,6'-F_2-bpy for X = 3; T = 2,2':6',2''-terpyridine) have been extensively studied[13, 15] and the accepted mechanism considers the key O-O bond forming step to be a water nucleophilic attack on a Ru^{V}-O moiety. Although this description is now widely accepted[16, 17] the corresponding deactivation pathways associated with this type of catalysts have not been reported. In this regard only the potential dissociation of bpy and subsequent oxidation to 2,2'-bipyridine *N, N*-dioxide has been pointed[18] out, as a hypothetical decomposition path.

Recently our group has found[19] that mononuclear complexes partially transform to dinuclear oxo bridge structures of general formula [TB-Ru^{IV}(μ-O)Ru^{IV}T(O)(H_2O)]$^{4+}$ (**X-dn**$^{4+}$; X = 1, 2 or 3), when high oxidation states are reached. The generation of these dinuclear complexes, involves necessarily the release of bpy from the first coordination sphere of the initial complex. The formed dinuclear complexes are active and rugged water oxidation catalysts and its presence complements the accepted mechanism, showing that the system is much more complex than originally described. Furthermore, the formation of these μ-O structures uncovers a tendency for the production of oxo-bridge oligomers by mononuclear Ru complexes in high oxidation states as it happens with Fe[2, 20] and Cu.[20-22]

In the present report we examine the interconnection between μ-oxo species generated after the chemical and electrochemical oxidation of mononuclear complexes related to [TB-Ru^{II}(H_2O)]$^{2+}$, **1**$^{2+}$, and discuss structural and electronic parameters.

2. Experimental section.

Materials. All reagents used in the present work were obtained from Aldrich Chemical Co. and were used without further purification. $RuCl_3 \cdot 3H_2O$ was supplied by Alfa Aesar and was used as received. Trifluoromethanesulfonic acid (HOTf) was pursued from CYMIT. Reagent-grade organic solvents were obtained from SDS and high-purity deionized water was obtained by passing distilled water through a nanopure Milli-Q water purification system.

Preparations.

$[Ru(trpy)(bpy)(H_2O)](PF_6)_2$ (**1**$^{2+}$),[23] $[Ru(trpy)(5,5'\text{-}F_2\text{-}bpy)(H_2O)](PF_6)_2$ (**2**$^{2+}$),[24] $[Ru(trpy)(6,6'\text{-}F_2\text{-}bpy)(H_2O)](PF_6)_2$ (**3**$^{2+}$),[24] $[(trpy)(bpy)Ru^{IV}(\mu\text{-}O)Ru^{IV}(trpy)(O)(H_2O)](ClO_4)_4$ (**1-dn**$^{4+}$)[19] and $[(trpy)(5,5'\text{-}F_2\text{-}bpy)Ru^{IV}(\mu\text{-}O)Ru^{IV}(trpy)(O)(H_2O)]\ (ClO_4)_4$ (**2-dn**$^{4+}$)[19] were prepared as described in the literature.

*$\{[Ru(trpy)(bpy)]_2(\mu\text{-}O)\}(ClO_4)_4 \cdot 7H_2O$ (**1-dm**$^{4+}$).* $[Ru(trpy)(bpy)(H_2O)](PF_6)_2$ (101.4 mg, 0.127 mmols) was dissolved in 0.1 M HOTf (127 mL). A amount of 100 equivalents of $(NH_4)_2Ce(NO_3)_6$ (7.10 g, 12.7 mmols) dissolved in the minimum amount of 0.1 M HOTf was added to the previous stirred solution. The solution is left stirred for approximately 1 week and UV-vis monitored periodically. When the band at 688 nm seemed to achieve a maximum value, a saturated aqueous solution of $NaClO_4$ (7 mL) was added. A dark green solid precipitated which was filtered and washed with some drops of cold water. The solid was collected and dried under vacuum overnight. Yield: 39.9 mg (45%). Anal. Calcd. for $C_{50}H_{50}Cl_4N_{10}O_{23}Ru_2$: C, 39.48; H, 3.45; N, 9.21. Found: C, 39.24; H, 3.24; N, 9.07.

Single crystal preparations.

*[(trpy)(6,6'-F_2-bpy)Ru^{IV}(μ-O)Ru^{IV}(trpy)(O)(H_2O)](ClO_4)$_4$·3H_2O (**3-dn^{4+}**).* Single crystals of **3-dn^{4+}** could be grown at RT one week after the addition of some drops of a sat. aq. $NaClO_4$ solution to a catalytic solution of **3^{2+}** in 0.1 M HOTf when oxygen evolution had finished.

*[(trpy)(bpy)Ru^{III}(μ-O)Ru^{III}(trpy)(CH_3CN)$_2$](PF_6)$_4$·H_2O·CH_3CN (**1-dn-N^{4+}**), [(trpy)(6,6'-F_2-bpy)Ru^{III}(μ-O)Ru^{III}(trpy)(CH_3CN)$_2$](PF_6)$_4$·CH_3CN (**3-dn-N^{4+}**).* **1-dn^{4+}** or **3-dn^{4+}**was dissolved in CH_3CN and approximately 10 μL of a sat. aq. solution of NH_4PF_6 were added. Crystals were grown by slow vapor diffusion of Et_2O into the solutions.

*{[Ru^{III}(trpy)(bpy)]$_2$(μ-O)}(ClO_4)$_4$·4H_2O (**1-dm^{4+}**).* Single crystals could be obtained at RT 2 days after the addition of some drops of a sat. aq. $NaClO_4$ solution to concentrated solutions of **1-dm^{4+}** in 0.1 M HOTf.

*{[$Ru^{III.5}$(trpy)(bpy)]$_2$(μ-O)}(ClO_4)$_4$·3/2H_2O (**1-dm^{5+}**).* Single crystals of **1-dm^{5+}** could be grown at RT 5 days after the addition of some drops of a sat. aq. $NaClO_4$ solution to a catalytic solution of **1-dm^{4+}** in 0.1 M HOTf when oxygen evolution had finished.

*{[Ru^{III}(trpy)(bpy)(μ-O)]$_2$$Ru^{IV}$(trpy)($H_2O$)}($ClO_4$)$_5$($PF_6$)·2$H_2O$ (**1-tr^{6+}**).* Single crystals for this complex were grown at RT 3 days after the addition of acetone to a solution of **1-dn^{4+}** in 0.1 M HOTf containing some drops of a sat. aq. solution of NH_4PF_6. The ratio acetone/water was approximately 1:1.

*{[Ru^{III}(trpy)(bpy)(μ-O)]$_2$$Ru^{IV}(pic)_2$}($ClO_4$)$_4$ (**1-tr-P^{4+}**).* A amount of 10 equivalents of picolinic acid was added to a catalytic solution of **1^{2+}** in 0.1 M HOTf when oxygen evolution had finished. The formation of **1-tr-P^{4+}** was tracked by the increase of a band at 688 nm in the UV-vis spectrum. Single crystals could be precipitated at RT 5 days after the addition of some drops of a sat. aq. NaClO4 solution to the above solution when the increase of the band was negligible.

{[(trpy)(5,5'-F_2-bpy)Ru^{III}(μ-O)Ru^{IV}(trpy)(CH_3COO)]$_2$(μ-O)}(ClO_4)$_6$·2H_2O (**2-tn-Ac^{6+}**), *{[(trpy)(bpy)Ru^{II}(μ-O)Ru^{IV}(trpy)(CH_3CN)]$_2$(μ-O)}(PF_6)$_6$·xCH_3CN* (**1-tn-N^{6+}**), and *{[(trpy)(6,6'-F_2bpy)Ru^{II}(μ-O)Ru^{IV}(trpy)(CH_3CN)]$_2$(μ-O)}(PF_6)$_4$(ClO_4)$_2$·3/2CH_3CN* (**3-tn-N^{6+}**). Single crystals for all these complexes could be obtained by the same procedure. The corresponding dinuclear compounds (**1-dn^{4+}**, **2-dn^{4+}** or **3-dn^{4+}**) were dissolved in CH_3CN and approximately 10 μL of a sat. aq. solution of NH_4PF_6 were added. Crystals were grown by slow vapor diffusion of Et_2O into the solutions.

Equipment and measurements. UV/Vis spectroscopy was performed on a Cary 50 (Varian) UV/Vis spectrophotometer in 1 cm or 0.2 cm when indicated quartz cuvettes. Cyclic voltammetry (CV) and differential pulse voltammetry (DPV) experiments were performed on an IJ-Cambria CHI-660 or a Bio-Logic SP-150 potentiostat using a three-electrode cell. Typical CV experiments were carried out at a scan rate of 100 mV s^{-1}. DPV experiments were carried out with the parameters: Pulses Height = 50 mV, Pulses Width = 50 ms, Step Height = 4 mV and Step Time = 200 ms. A glassy carbon electrode (3 mm diameter) was used as working electrode, platinum wire as auxiliary electrode, and SSCE as a reference electrode. Working electrodes were polished with 0.05 micron alumina paste, and rinsed with distilled water and acetone followed by blow-drying before each measurement. All cyclic voltammograms presented in this work were recorded in the absence of light and inside a Faradaic cage. The electrochemical experiments were carried out in 0.1 M CF_3SO_3H (pH 1.0). $E_{1/2}$ values reported in this work were estimated from CV experiments as the average of the oxidative and reductive peak potentials ($E_{p,a}$ + $E_{p,c}$)/2 or taken as E(I_{max}) from DPV measurements.

A 400 MHz Bruker Avance II spectrometer and a Bruker Avance 500 MHz were used to carry out NMR spectroscopy at room temperature. Samples were run in 0.1 M DOTf or CD_3CN with

internal references (residual protons). Elemental analysis was performed using an EA-1108, CHNS-O elemental analyzer from Fisons Instruments.

Samples for resonance Raman spectroscopy were prepared typically by mixing a 1 mM solution of the starting complex with the desired amount of $(NH_4)_2Ce(NO_3)_6$ and transferring 100 μL of the reaction solution to a aluminium crucible and subsequently frozen at appropriate times in liquid N_2. Then, the crucible was placed into a Linkam THMS 600 temperature controlled cryo stage to keep the temperature at -12°C. The rR spectrum was acquired using a Renishaw inVia Reflex RAMAN confocal microscope (Gloucestershire, UK), equipped with an Ar-ion laser at 514 nm and a Peltier-cooled CCD detector (-70°C) coupled to a Leica DM-2500 microscope. Calibration was carried out daily by recording the Raman spectrum of an internal Si standard. Rayleigh scattered light was appropriately rejected by using edge-type filters. Spectrums were recorded with the accumulation of 5 scans with a 20 s scan time each one. A 10x working distance microscope objective was used to focus 50% of the laser power (25 mW) onto the sample.

On-line manometric O_2 measurements were carried out on a Testo 521 differential pressure manometer with an operating range of 1-100 hPa and accuracy within 0.5 % of the measurement. The manometer was coupled to thermostated reaction vessels for dynamic monitoring of the headspace pressure above each reaction. The manometer's secondary ports were connected to thermostated reaction vessels containing the same solvents and headspace volumes as the sample vials. A typical experiment consists in the addition of 100 equivalents of $(NH_4)_2Ce(NO_3)_6$ previously dissolved in 100 μL of 0.1 M HOTf upon a solution of the catalyst in 1.850 mL of the same solvent containing the suitable amount of complex to yield 1 mM final concentration. This combination is termed catalytic solution.

Single-Crystal X-Ray Structure Determination. All measured crystals were prepared under inert conditions immersed in perfluoropolyether as the protecting oil for manipulation.

Data collection. Crystal structure determination was carried out using a Apex DUO Kappa 4-axis goniometer equipped with an APPEX 2 4K CCD area detector, a Microfocus Source E025 IuS using MoK_α radiation, Quazar MX multilayer Optics as monochromator and an Oxford Cryosystems low temperature device Cryostream 700 plus (T = -173 °C). Full-sphere data collection was used with ω and φ scans. Programs used: Data collection APEX-2,[25] data reduction Bruker Saint V/.60A.[26]

Structure solution and refinement. Crystal structure solution was achieved using direct methods as implemented in SHELXTL[27] and visualized using the program XP. Missing atoms were subsequently located from difference Fourier synthesis and added to the atom list. Least-squares refinement on F^2 using all measured intensities was carried out using the program SHELXTL. All non hydrogen atoms were refined including anisotropic displacement parameters. In the case of **1-tn-N^{6+}** the program SQUEEZE[28] was applied in order to avoid the highly disordered solvent molecules leading to a refined model with a R1 value of 6.34 % in which all the solvent molecules were removed. The crystals obtained for **1-tn-N^{6+}** were diffracting extremely weak so that only a completeness of 93.6 % could be reached at a resolution of sin(theta/lambda) = 0.6. Compound **1-dm^{4+}** crystallized as a two domain crystal (ratio 73:27). The collected data were processed with TWINABS taking in account overlapping reflections.

3. Results and discussion.

3.1. Synthesis.

In a previous report[19] we have demonstrate that addition of an excess of Ce(IV) to the water oxidation catalyst $[TB\text{-}Ru^{II}(H_2O)]^{2+}$, $\mathbf{1}^{2+}$, generates oxygen and that during turnover the **bpy** ligand slowly falls off the first coordination sphere and generates $[T\text{-}Ru^{VI}(O)_2(H_2O)]^{2+}$. The latter in turn reacts with $\mathbf{1}^{2+}$, to form the dinuclear complex, $\mathbf{1\text{-}dn}^{4+}$, as indicated below and in Scheme 1,

$$[TB\text{-}Ru^{II}\text{-}OH_2]^{2+}\ (\mathbf{1}^{2+}) \ + \ [T\text{-}Ru^{VI}\text{-}(O)_2OH_2]^{2+} \rightleftharpoons [TB\text{-}Ru^{IV}\text{-}O\text{-}Ru^{IV}\text{-}(T)(O)OH_2]^{2+}\ (\mathbf{1\text{-}dn}^{4+}) \ + \ H_2O \quad (1)$$

One electron oxidation of $\mathbf{1\text{-}dn}^{4+}$ produces a dinuclear complex in oxidation state IV,V that is associated with a large electrocatalytic wave responsible for water oxidation. On the other hand the $\mathbf{1\text{-}dn}^{4+}$ complex is also a very strong oxidative reagent specially towards organic substrates. For instance, addition of MeCN produces the immediate reduction of the dimer to lower oxidation states III,III followed by solvent coordination. The latter is indicated in the equation below,

$$[TB\text{-}Ru^{III}\text{-}O\text{-}Ru^{III}\text{-}T(OH_2)_2]^{4+} \ + \ 2\ MeCN \ \rightarrow [TB\text{-}Ru^{III}\text{-}O\text{-}Ru^{III}\text{-}T(MeCN)_2]^{4+}\ (\mathbf{1\text{-}dn\text{-}N}^{4+}) \ + \ 2H_2O \quad (2)$$

and maintaining the original Ru-O-Ru backbone. In an analogous manner, addition of ether/MeCN produces tetranuclear complexes in different oxidation states. As in the previous case, the addition of organic compounds give rise to the immediate reduction of the initial dinuclear complex, $\mathbf{X\text{-}dn}^{4+}$, followed by an oligomerization process generating,

We have also found qualitative evidence that the dinuclear complex **1-dn**$^{4+}$, could be obtained electrochemically after an applied potential of 1.2 V overnight from a solution of **1**$^{2+}$. This indicates the existence of multiple routes to prepare the dinuclear complexes from their respective mononuclear ones and is in agreement with Ce(IV) acting only as an outer sphere electron transfer agent.

$$[TB\text{-}Ru^{III}\text{-}O\text{-}TRu^{IV}(H_2O)\text{-}O\text{-}TRu^{IV}(H_2O)\text{-}O\text{-}Ru^{III}\text{-}TB]^{8+}\ (\mathbf{1\text{-}tn^{8+}}) + 2\ AcO^- \rightarrow$$

$$[TB\text{-}Ru^{III}\text{-}O\text{-}TRu^{IV}(AcO)\text{-}O\text{-}TRu^{IV}(AcO)\text{-}O\text{-}Ru^{III}\text{-}TB]^{6+}\ (\mathbf{1\text{-}tn\text{-}Ac^{6+}}) + 2H_2O \quad (3)$$

where the acetate ligand coordinates in a monodentate terminal fashion. The origin of the acetato ligand is not clear but might come from the hydrolysis of MeCN catalyzed by Ru complexes as we and others have shown previously.[29,30]

Further reduction of **1-tn**$^{8+}$ and solvent coordination yields the tetranuclear complexes, **X-tn-N**$^{6+}$, as indicated below,

$$[TB\text{-}Ru^{III}\text{-}O\text{-}TRu^{IV}(H_2O)\text{-}O\text{-}TRu^{IV}(H_2O)\text{-}O\text{-}Ru^{III}\text{-}TB]^{8+}\ (\mathbf{1\text{-}tn^{8+}}) + 2\ MeCN + 2e^- \rightarrow$$

$$[TB\text{-}Ru^{II}\text{-}O\text{-}TRu^{IV}(MeCN)\text{-}O\text{-}TRu^{IV}(MeCN)\text{-}O\text{-}Ru^{II}\text{-}TB]^{6+}\ (\mathbf{1\text{-}tn\text{-}N^{6+}}) + 2H_2O \quad (4)$$

Addition of acetone to the initial dinuclear complex, **1-dn**$^{4+}$, produces an immediate reduction followed by the oligomerization process that in this case generates the trinuclear complex , [TB-Ru^{III}-O-TRu^{IV}(H$_2$O)-O-Ru^{III}-TB]$^{6+}$, **1-tr**$^{6+}$, where the Ru-aqua ligands is maintained thanks to the weak coordination capacity of acetone. In an analogous manner, addition of picolinic acid to a solution of **1-dn**$^{4+}$ generates the formation of a trinuclear complex **1-tr-P**$^{6+}$, with similar structure as **1-tr**$^{6+}$, but where the [T-Ru-(H$_2$O)-O] moiety has been substituted by the [P$_2$-Ru-O] group.

Finally, in the presence of bpy but in the absence of organic substrates the IV,IV oxidation state slowly decays (about 1 week) to lower oxidation states giving complexes such as the dimer, $[TB\text{-}Ru^{III}\text{-}O\text{-}Ru^{III}\text{-}TB]^{4+}$, **1-dm^{4+}**, in 85 % yield, whose formation can be monitored by UV-vis spectroscopy (see sup. inf.) thanks to the presence of a highly characteristic band at 688 nm as depicted in Figure 3.

All the above synthetic results combined point out the existence of an oligomerization process where the [T-Ru-(H_2O)-O] moiety acts as a repeating unit whereas the [TB-Ru] moiety acts as a stopper to the polymerization process, that is,

$$n\ [T\text{-}Ru^{IV}\text{-}(O)(OH_2)_2]^{2+} \rightarrow [T\text{-}Ru^{IV}\text{-}(O)OH_2]_n^{2n+} + n\ H_2O \quad (5)$$

$$2\ [TB\text{-}Ru^{III}\text{-}OH_2]^{3+} + [T\text{-}Ru^{IV}\text{-}(O)OH_2]_n^{2n+} \rightarrow \{TB\text{-}Ru\text{-}[O\text{-}TRu(H_2O)]_n\text{-}O\text{-}Ru\text{-}TB\}^{(2n+4)+} + 2H^+ + H_2O \quad (6)$$

Depending on time and solubility oligomers with a different number of repeating units are obtained.

Scheme 1. Synthetic strategy and complex nomenclature. X=1 for unsubstituted bpy, X = 2 for 5,5'-F_2-bpy, and X = 3 for 6,6'-F_2-bpy. Color codes for formal Ru oxidation states: VI, fuchsia; IV, blue; III, green; II, orange.

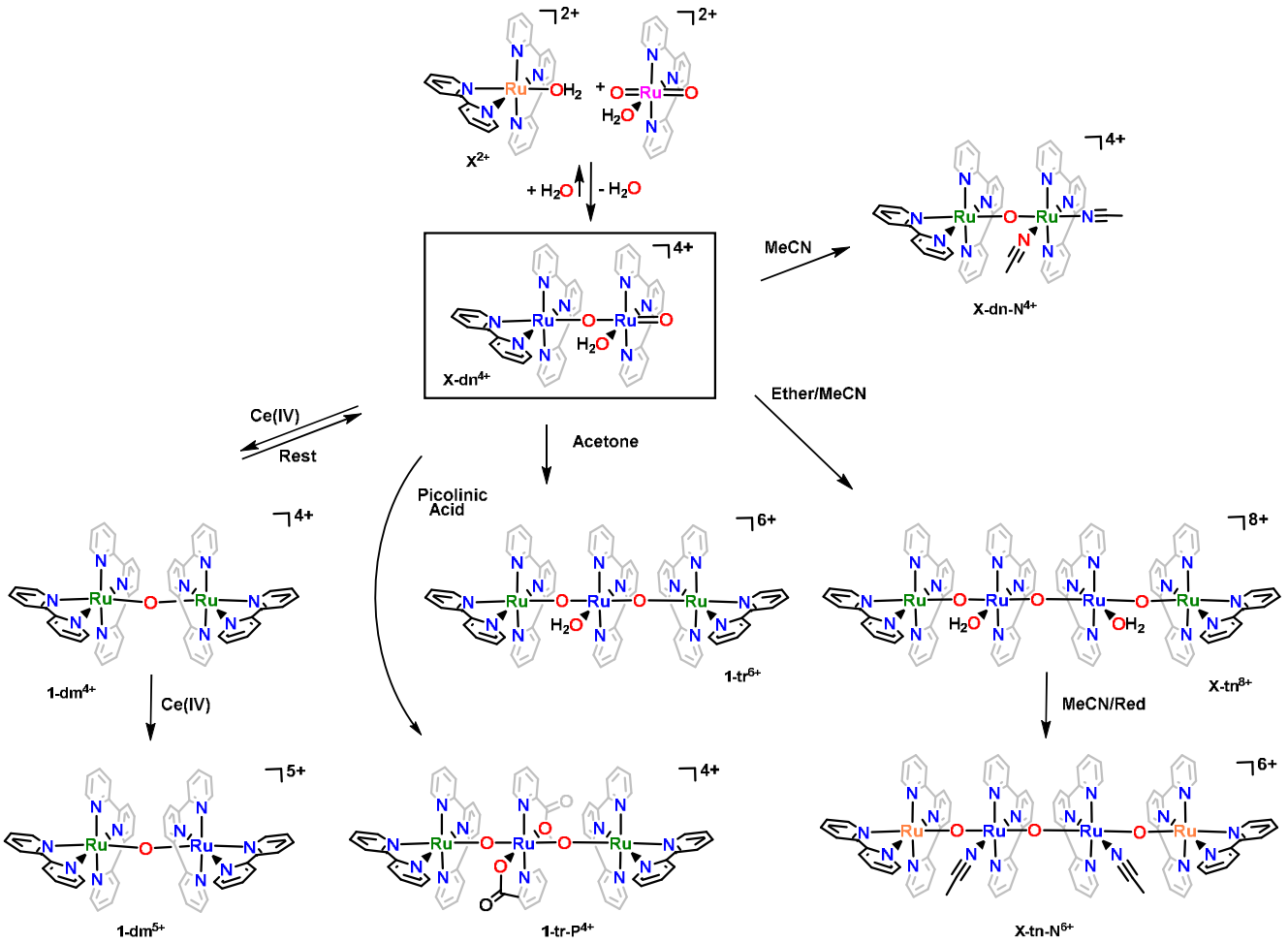

3.2. RuORu Structure and electronic properties.

The crystal structure of all the Ru oxo bridged complexes discussed in the present work are displayed in Figure 1. In all cases the metal center exhibits a distorted octahedral coordination and the most interesting features of these complexes are their Ru-O-Ru bond distances and angles that are summarized in Table 1 together with related oxo-bridged Ru complexes previously reported in the literature.

The RuORu bonding parameters depend on the oxidation state as well as on the degree of electronic coupling between the metal centers through the oxygen bridging atom. A qualitative MO diagram for π -system of the RuORu type of complexes[31, 32] is shown in Figure 2 and sheds some light into the orbitals involved in this type of bonding for the RuORu moiety

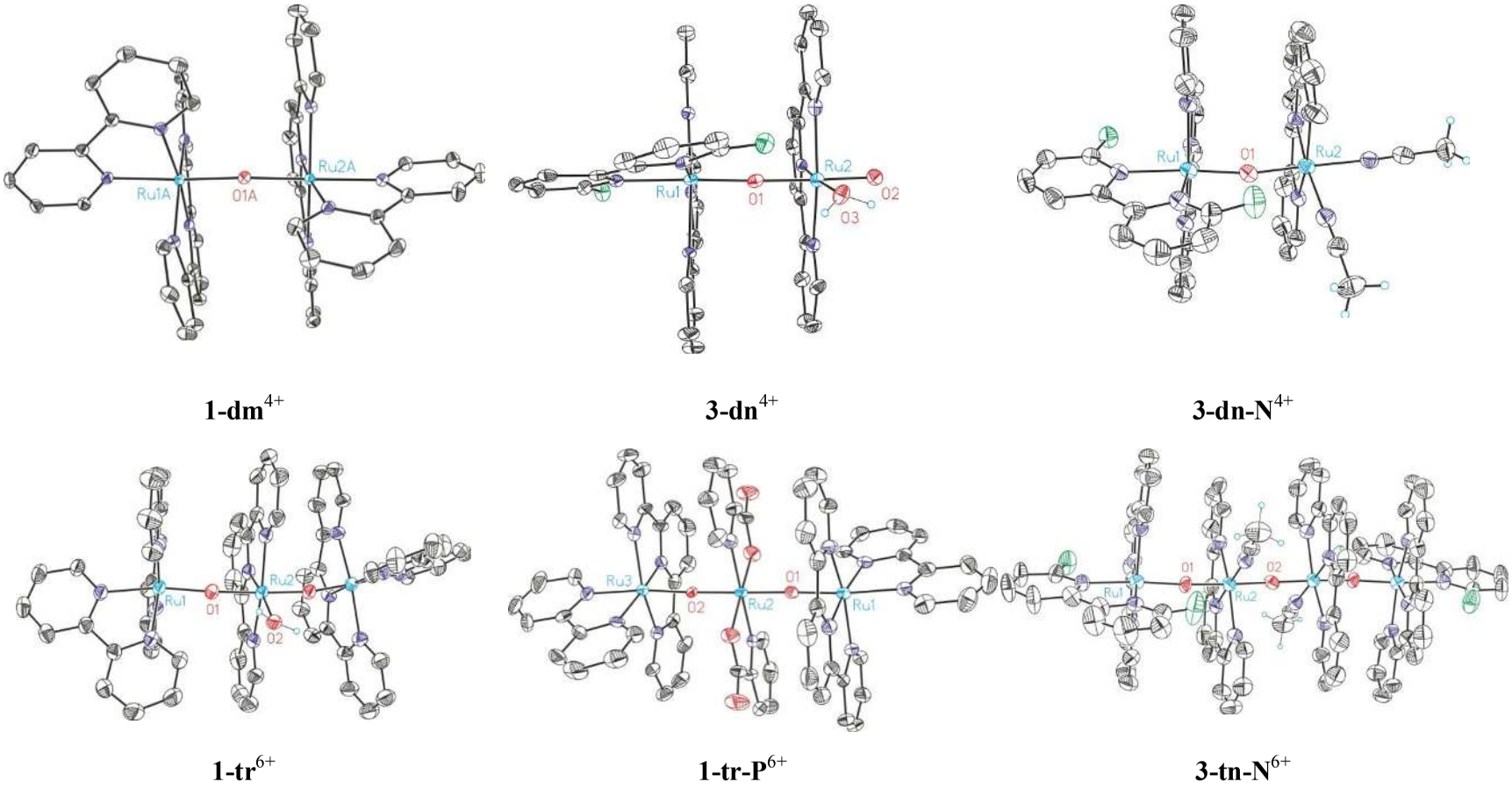

1-dm^{4+} **3-dn**$^{4+}$ **3-dn-N**$^{4+}$

1-tr^{6+} **1-tr-P**$^{6+}$ **3-tn-N**$^{6+}$

Figure 1. Ortep plot (ellipsoid drawn at 50 % probability) of the X-ray structures. Color codes: Ru, cyan; O, Red; N, Blue; C, black; F, green. H atoms are not shown except for monodentate ligands.

Table 1. Comparison of important bond distances (Å) and angles (deg) for oxo-bridge polynuclear metal complexes.

Complex[a]	Ru(2)-O(2)	Ru(2)-O(1)	Ru(1)-O(1)	Ru(1)-O-Ru(2)	Ref.
Ru^{IV}-O_1-Ru^{IV}					
1-dn^{4+}	1.747(3)[b]	1.832(3)	1.848(3)	175.43(18)	Tw.[d]
2-dn^{4+}	1.738(4)[b]	1.830(3)	1.855(3)	171.5(2)	Tw.
3-dn^{4+}	1.731(3)[b]	1.833(3)	1.850(3)	172.63(16)	Tw.
$\{[(OEP)ClRu^{IV}]_2O\}$[c]		1.793(2)	1.793(2)	180	[36]
$\{[(OEP)(OH)Ru^{IV}]_2O\}$[c]		1.847(13)	1.847(13)	180	[37]
$\{[Cl_5Ru^{IV}]_2O\}^{4-}$[c]		1.80	1.80	180	[38]
Ru^{III}-O_1-Ru^{IV}					
1-dm^{5+}		1.846(2)	1.848(2)	169.90(13)	Tw.
$[(bpy)_2(H_2O)Ru^{III}ORu^{IV}(OH)(bpy)_2]^{4+}$		1.847(12)	1.823(12)	170.0(7)	[35]
$[(bpy)_2(Cl)Ru^{III}ORu^{IV}(Cl)(bpy)_2]^{4+}$		1.845(9)	1.805(9)	170.7(5)	[35]
$[(TACN)Ru^{III}(O)(CH_3CO_2)_2Ru^{IV}(TACN)]^{3+}$		1.849(5)	1.837(5)	130.1(3)	[33]
Ru^{III}-O_1-Ru^{III}					
1-dn-N^{4+}[e]		1.864(4)[f]	1.865(4)	169.9(2)	Tw.
3-dn-N^{4+}		1.912(5)[f]	1.891(5)	166.1(3)	Tw.
1-dm^{4+}		1.8810(12)	1.8819(12)	164.31(7)	Tw.
$\{[Ru^{III}(trpy)(C_2O_4)]_2(\mu\text{-}O)\}$		1.846(8)	1.841(8)	148.5(4)	[51]
$\{[Ru^{III}(TACN)(acac)]_2(\mu\text{-}O)\}^{2+}$		1.913(1)	1.913(1)	180.0(1)	[47]
$\{[Ru^{III}(bpy)_2(NH_3)]_2(\mu\text{-}O)\}^{4+}$		1.894(2)	1.894(2)	158.2(4)	[52]
$\{[Ru^{III}(bpy)_2(H_2O)]_2(\mu\text{-}O)\}^{4+}$		1.869(1)	1.869(1)	165.4(3)	[53]
$\{[Ru^{III}(bpy)_2(NO_2)]_2(\mu\text{-}O)\}^{2+}$		1.876(6)	1.890(7)	157.2(3)	[54]
$\{[Ru^{III}(TACN)]_2(\mu\text{-}O)(\mu\text{-}CH_3CO_2)_2\}^{2+}$		1.884(2)	1.884(2)	119.7(2)	[33]
$\{[Ru^{III}(tpm)]_2(\mu\text{-}O)(\mu\text{-}O_2P(O)(OH))_2\}$		1.868(2)	1.868(2)	124.7(4)	[32]

M^{III}-O_1-Ru^{IV}-O-M^{III}[g,h]					
1-tr-P^{4+}[l]		1.805(5), 1.799(5)[i]	1.872(5), 1.875(5)[j]	173.5(3), 176.6(3)[k]	Tw.
1-tr^{6+}		1.821(3)[i]	1.881(3)[j]	166.0(2)[k]	Tw.
$\{[(NH_3)_5Ru^{III}(\mu\text{-}O)]_2Ru^{IV}(en)_2\}^{6+}$		1.850(4)[i]	1.891(4)[j]	177.2(4)[k]	[55]
$\{[(BuNH_2)((DPG)BF_2)_2Fe^{III}(\mu\text{-}O)]_2Ru^{IV}(TPP')\}$[l]		1.796(8), 1.801(8)[i]	1.786(8), 1.788(8)[j]	174.8(5), 175.1(5)[k]	[41]
$\{[(Salmah)Fe^{III}(\mu\text{-}O)]_2Ru^{IV}(TPP)\}$		1.866(6)[i]	1.848(6)[j]	155.2(5)[k]	[56]
Ru_1^{II}-O_1-Ru_2^{IV}-O_2-Ru^{IV}-O-Ru^{II}[g]					
1-tn-N^{6+}	1.8496(3)	1.839(2)	1.883(2)	169.67(15)	Tw.
2-tn-Ac^{6+}	1.8364(3)	1.823(2)	1.865(3)	169.44(16)	Tw.
3-tn-N^{6+}	1.8378(8)	1.829(6)	1.892(6)	168.10(4)	Tw.

[a]Ligand abbreviation: OEP = octaethylporphinate, TACN = 1, 4, 7-trimethyl-1, 4, 7-triazacyclononane, acac = pentane-2,4-dionate, en = ethylenediamine, $BuNH_2$ = *n*-butylamine, $(DPG)BF_2$ = (difluoroboryl)-diphenylglyoximate, TPP' = tetrakis(4-methoxyphenylporphyrinate), Salmah = *N,N'*-(4-methyl-4-azaheptane-1,7-diyl)bis(salicylaldiminaate), TPP = 5,10,15,20-tetraphenylpophyrinate. [b] Ru(2) corresponds to Ru bound to the oxo terminal ligand which is labeled as O(2). [c] High symmetry complexes with $Ru(1)\text{-}O_{bridge} = Ru(2)\text{-}O_{bridge}$. [d]This work. [e]The bipyridine and the acetonitrile ligands are disordered interchanging its positions with a ratio of 86:14 which means that Ru(1) and Ru(2) also do it. [f]Ru(2) corresponds to Ru bound to two CH_3CN ligands. [g]Usually centrosymmetric complexes [h]M(III) = Ru(III) in **1-tr-P^{4+}** and **1-tr^{6+}** and M(III)=Fe(III) in the remaining complexes. [i]Ru(2) corresponds to the central Ru(IV) atom. [j]Ru(1) corresponds to the outer M(III) atoms. [k]Ru(IV)-O-M(III) angle. [l]The complex is non-centrosymmetric, so that a couple of distances or angles are showed in each field.

Here the Ru-O bond is taken as the z axis and thus the d_{xz} and d_{yz} orbitals from the metal atoms mix with two π-type p orbitals from the oxo brigding atom producing three sets of bridge-based orbitals. The first set consists of bonding orbitals (π_1^b, π_2^b) which have a large p_O character. The next set contains two non-bonding or slightly antibonding orbitals (π_1^{nb}, π_2^{nb}) which have a large $d\pi_{Ru}$ character. Finally, the third set comprises two antibonding orbitals (π_1^*, π_2^*) which have also a large $d\pi_{Ru}$ character. For complexes with a linear geometry, that is with a RuORu angle of 180° π_1^* and π_2^* are degenerate. However when the RuORu angles are smaller than 180°, the degeneracy is lost and their energy difference is a function of the RuORu angle.

As a consequence of this, the electronic configuration of the dinuclear oxo bridge d^5 Ru(III) complexes will be a function of the RuORu angle since the π* orbitals are now populated. If the energy gap between π_1^* and π_2^* is sufficiently large then the electronic configuration is $(\pi_1^b)^2$ $(\pi_2^b)^2$ $(\pi_1^{nb})^2$ $(\pi_2^{nb})^2$ $(\pi_1^*)^2$, and thus the complexes will be diamagnetic. This is actually the case for $\{[Ru^{III}(TACN)]_2(\mu\text{-}O)(\mu\text{-}CH_3CO_2)_2\}^{2+}$[33] and $\{[Ru^{III}(tpm)]_2(\mu\text{-}O)(\mu\text{-}O_2P(O)(OH))_2\}$[32] with RuORu angles of 120° and 125° respectively. In contrast, dinuclear oxo bridge d^5 Ru(III) complexes with RuORu angles close to 180° display a paramagnetic behavior due either the degeneracy of π_1^* and π_2^* or because they are very close in energy and thus both will be populated at RT.

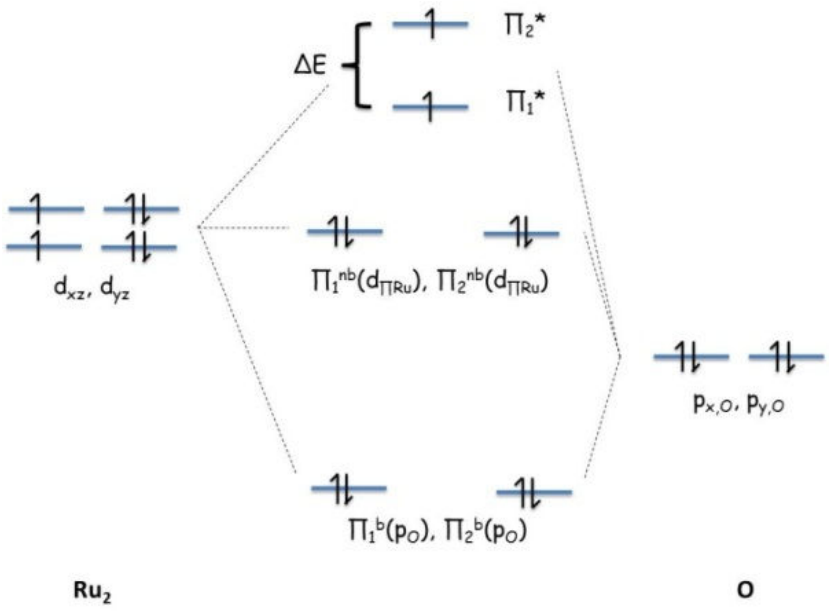

Figure 2. Qualitative MO diagram for the π system of Ru-O-Ru complexes. ΔE depends on the angle of the moiety, the smaller the angle the larger the energetic separation. The electronic configuration illustrates the case of a d^5-d^5 Ru(III)-O-Ru(III) complex with a linear angle (180°).

For the case of **1-dm**$^{4+}$, the Ru-O-Ru angle is 164° and thus has a paramagnetic behavior at RT that is manifested by the broad range of the chemical shift (-30 to +30 ppm) where the resonances are observed in the 1H-NMR spectrum (see sup inf). A similar shift has been observed for related Ru^{III}-O-Ru^{III} complexes.[34] The number of signals agrees with two symmetric [Ru(trpy)(bpy)] halves manifesting the existence of symmetry in solution.

For the one electron oxidized complex, **1-dm**$^{5+}$, the Ru-O distance is shortened by approximately 0.035 Å, in agreement with a higher bond order for Ru-O because of the removal of an electron from the antibonding orbital π_2* if compared to **1-dm**$^{4+}$. In addition the two Ru-O

bonds in **1-dm**$^{5+}$ are almost identical suggesting a high degree of electronic coupling between the two Ru metal centers through the oxo bridge.

The dinuclear complexes **1-, 2- and 3-dn**$^{4+}$ have two radically different sites; while one of them contains a [TB-Ru^{IV}] moiety the other one is a [TRu^{IV}(O)(H2O)]. This is manifested in the non-symmetric nature of the Ru-O-Ru bonds as can be observed in Table 1. The same effect has been also found in the III,IV form of the blue dimer[35].

This is in sharp contrast with previous reported[36-38] symmetric complexes where the Ru^{IV}-O-Ru^{IV} bonds are practically identical (**Table 1**). Finally in the crystal structure of **3-dn**$^{4+}$ we find the shortest Ru-O terminal bond ever reported.[39]

The Ru^{IV}-O-Ru^{IV} angles are slightly bent with respect to the ideal 180˚ found in previously reported complexes, because the steric constraint due the proximity of the bpy ligand to the aquo group. In this way the less sterically demanding bpy in **1-dn**$^{4+}$ generates a RuORu angle of 175.5˚, whereas in the more sterically demanding Fluoro-bpys are 171.5^{o} in **2-dn**$^{4+}$ and 172.6^{o} in **3-dn**$^{4+}$.

A related structural motif is found for complexes **1-dn-N**$^{4+}$ and **3-dn-N**$^{4+}$ (Figure 1 and Supp Inf. and Table 1) where the aqua group have been replaced by MeCN and the Ru metal centers are at oxidation state III. As a consequence of this, the Ru-O bond distances are slightly elongated. (See Table 1).[35]

Two trinuclear complexes with a Ru^{III}-O-Ru^{IV}-O-Ru^{III} backbone have been obtained, **1-tr**$^{6+}$ and **1-tr-P**$^{4+}$, (see Figure 1) and whose structures are reminiscent of Ruthenium Red,[40] {[(NH$_3$)$_5$Ru^{III}(μ-O)]$_2$[μ-Ru^{IV}(NH$_3$)$_4$]}$^{6+}$. There are only a few crystallographically characterized trinuclear Ru-oxo-bridged complexes including some heterotrinuclear ones,[41] where the Ru is situated at the central position in oxidation state IV.(See Table 1)

In **1-tr**$^{6+}$ the central Ru atom adopts a *trans* dioxo arrangement and bears an aquo ligand. The Ru^{IV}-O and the Ru^{III}-O distances are significantly different suggesting a weak coupling among metallic atoms. (Table 1) The *trans*-dioxo nature of the central Ru together with the presence of the aqua ligand attached to the same metal center converts it into a potentially powerful WOC.[19]

The main structural parameters for **1-tr-P**$^{4+}$ are also collected in Table 1. As in the previous case the Ru^{IV}-O distance is considerably shorter than that of Ru^{III}-O (Δd = 0.078 Å) suggesting again a weak electronic coupling. It is worth mentioning that the Ru^{IV}-$O_{Carboxylate}$ bond (2.034 Å) is shorter than that reported[42-44] for mononuclear picolinate Ru(II) complexes (2.085-2.102 Å) and similar to that of a described[45] in a Ru(IV) piridinecarboxylate compound (2.068(3) Å), supporting the oxidation state assignment.

Tetranuclear complexes **1-tn-N**$^{6+}$ and **3-tn-N**$^{6+}$ with the Ru_1^{II}-O_1-Ru_2^{IV}-O_2-$Ru_{2'}^{IV}$-$O_{1'}$-$Ru_{1'}^{II}$ backbone have also been obtained and their Orteps are presented in Figure 1 and the sup inf, whereas selected bond distances and angles are displayed in Table 1.

These complexes contain an inversion center, "*i*", situated at the central O_2 atom. For complex **1-tn-N**$^{6+}$ the Ru_1-O distance is 1.88 Å that is significantly longer than the Ru_2-O distances that are 1.85 and 1.84 Å. This Ru-O bonding distances advocate for a [(Ru^{II}-O-Ru^{IV})$_2$-(μ-O)] assignment rather than a [(Ru^{III}-O-Ru^{III})$_2$-(μ-O)] which would also be in agreement with the overall charge of the cationic part of the molecule. A similar analysis can be carried out for **3-tn-N**$^{6+}$. However the two electron oxidized complex **3-tn-Ac**$^{6+}$, where in addition the MeCN ligands have been substituted by acetate acting as a monodentate ligand, have similar Ru_2-O distances but slightly shorter Ru_1-O, and thus support a [(Ru^{III}-O-Ru^{IV})$_2$-(μ-O)] assignment. In turn this also support the [(Ru^{II}-O-Ru^{IV})$_2$-(μ-O)] assignment for **1-tn**$^{6+}$ and **3-tn**$^{6+}$ as opposed to

intermediate oxidation state options such as [($Ru^{II.5}$-O-$Ru^{III.5}$)$_2$-(μ-O)], although further spectroscopic analysis is needed for complete oxidation state characterization.

3.3. The chemistry related to 1-dm^{4+}.

As mentioned in the synthetic section **1-dm**$^{4+}$ can be obtained in high yield by adding 100 equivalents of Ce(IV) to a 0.1M triflic acid aqueous solution containing 1 equivalent of **1**$^{2+}$. As reported earlier[19] this generates a system containing two parallel catalytic systems based on the oxidation of **1**$^{2+}$ and the formation of **1-dn**$^{4+}$ arising from bpy loss from the former, as indicated in equation 1. Once Ce(IV) is depleted the two catalytic cycles stop generating species at high oxidation states such as [trpy-bpy-Ru^{IV}=O]$^{2+}$ and **1-dn**$^{4+}$. These species are not stable in acidic solution and decay slowly to lower oxidation state species in the presence of free bpy. Over a period of one week this mix decays mainly to the formation of **1-dm**$^{4+}$ in 85 % yield judging from UV-vis.

Complex **1-dm**$^{4+}$, has been characterized in solution by UV-vis and NMR spectroscopy and in the solid state by X-ray diffraction analysis as shown in Section 3.2. In addition the complex has been characterized electrochemically by means of CV and DPV and its reactivity tested upon addition of a large excess of Ce(IV).

The UV-vis spectrum of **1-dm**$^{4+}$ in a 0.1 M trilfic acid solution is displayed in Figure 3. The most interesting feature of this spectrum is the band at 688 nm typical of Ru^{III}-O-Ru^{III} type of complexes[46, 47] which is associated with the overlapping of MLCT and bridge-based transitions.[48, 49] Interestingly the oxidation of the mononuclear complexes **1**$^{2+}$ and **2**$^{2+}$ with only 2 or 3 equivalent of Ce(IV) also produces this band manifesting the tendency toward oxo-bridge formation of mononuclear systems. The ^{1}H-NMR at RT for the paramagnetic complex **1-dm**$^{4+}$ was also registered in 0.1 M CF_3SO_3D in D_2O. The spectrum shows resonances in a very wide

range due to the paramagnetic shift exerted by the Ru(III) d^5 ions. A DOSY experiment was also carried out that nicely reflects that the hydrodynamic radius, according to the Stokes-Einstein equation is 1.9 times larger than for $[Ru(trpy)(bpy)(CH_3CN)]^{2+}$, used as a mononuclear standard.

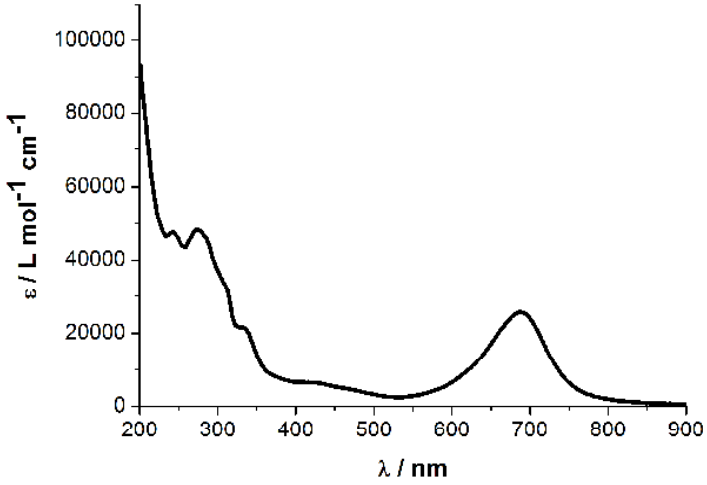

Figure 3. UV-vis spectrum of **1-dm**$^{4+}$ in 0.1 M HOTf.

The CV of **1-dm**$^{4+}$ in 0.1 M trilfic acid is depicted in Figure 4. The initial anodic scan from the open circuit potential up to 1.40 V shows a reversible wave at $E_{1/2}$ = 1.08 V (ΔE = 55 mV). This electrochemical process is attributed to the one electron oxidation in eq. 1, according to previously reported[46, 47] related complexes.

$$Ru^{III}\text{-}O\text{-}Ru^{III} - 1e^- \rightarrow Ru^{III}\text{-}O\text{-}Ru^{IV} \qquad E_{1/2} = 1.08\ V \qquad (7)$$

After a subsequent cathodic scan until 0 V a chemically irreversible wave appears at $E_{p,c}$ = 0.22 V which is consistent with the 2 $e^-/1H^+$ transfer as indicated in equation 8, and similarly reported in the literature for related complexes, followed by Ru-O bond breaking and formation of the mononuclear complex $\mathbf{1}^{2+}$,

$$Ru^{III}\text{-}O\text{-}Ru^{III} + 2e^- + H^+ \rightarrow Ru^{II}\text{-}(OH)\text{-}Ru^{II} \qquad E_{p,c} = 0.22\ V \qquad (8)$$

$$Ru^{II}\text{-}(OH)\text{-}Ru^{II} + H_2O + H^+ \rightarrow 2\ Ru^{II}\text{-}OH_2 \qquad (9)$$

This is nicely seen in the second CV cycle where a new chemically reversible and an electrochemically quasireversible waves appears at E^0 = 0.82 V and E^0 = 0.98 V respectively, which are associated with $\mathbf{1}^{2+}$.

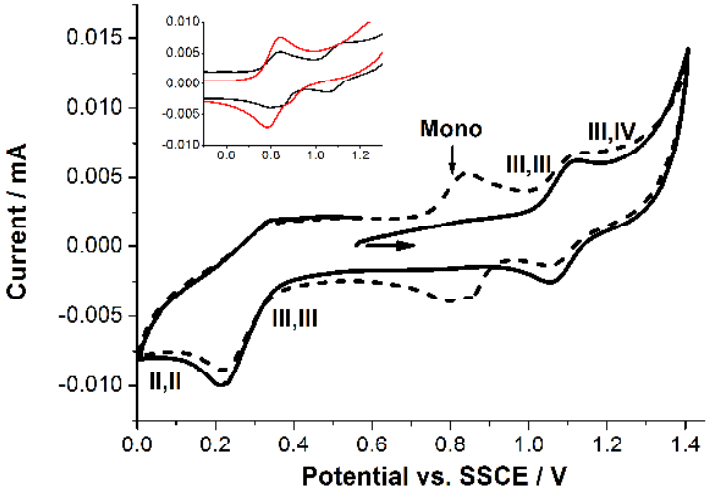

Figure 4. CV of **1-dm**$^{4+}$ in 0.1 M HOTf, 1st cycle (solid line), 2nd cycle (dashed line). The inset shows a comparison of the second cycle (black) and a CV from a solution of $\mathbf{1}^{2+}$ (red) in the same solvent. Polished glassy carbon was used as working electrode, a Pt wire as counter electrode and SSCE as reference electrode. Scan rate = 100 mV s^{-1}.

Addition of 100 equivalents of Ce(IV) to **1-dm**$^{4+}$ generates oxygen with a TN of 7.6 and a TOF_i of 6.19 h^{-1} as can be extracted from the oxygen generation profile as a function of time that is presented in the Sup Inf. This was a surprising result since given the absence of an aqua group bonded to the Ru metal it was not expected to be an active WOC. In order to decipher what were the active species we followed the reaction by rR spectroscopy.

Figure 5 shows the rR spectrum of **1-dm**$^{4+}$ in 0.1 M triflic acid before the addition of Ce(IV) in a black line. After addition of Ce(IV) two spectra were recorded one after 30 s (red line) and the second one after 2.73 h (blue line). First, a vibration with high intensity at 392 cm^{-1} observed in **1-dm**$^{4+}$ before oxidant addition, due to the ν_S Ru-O-Ru mode,[35, 49, 50] shifts to 404 cm^{-1}. This blue shift is in agreement with a higher bond order of the Ru-O-Ru moiety and thus can be associated with the one electron oxidation of the initial dimer to form **1-dm**$^{5+}$. Incidentally addition of a large amount of ClO_4^- to this solution generates nice brown crystals of **1-dm**$^{5+}$, that confirm this assignment. Secondly and surprisingly both spectra at 30 s and at 2.73 h present a vibration at 801 cm^{-1} which is the typical signature of **1-dn**$^{4+}$, as we have reported earlier.[19] This clearly suggest that upon addition of Ce(IV) the **1-dm**$^{4+}$ dimer partially reorganizes to form a small amount of **1-dn**$^{4+}$, which in turn is responsible for the observed catalytic oxygen generation, as we have demonstrated earlier. No RuO_2 was detected in our experiments which is in agreement with the oxidative robustness of the ligands used and the stability of the Ru-oxo-bridged moiety. The formation of RuO_2 as a black solid is very obvious when using Ru complexes with ligands that are easy to oxidize, typically containing benzyllic, pyridylbenzyllic or amine type of groups.[57,58] We also have a nice correlation of dimer formation and oxygen generation[19] that again is in agreement with the absence of RuO_2 in our systems.

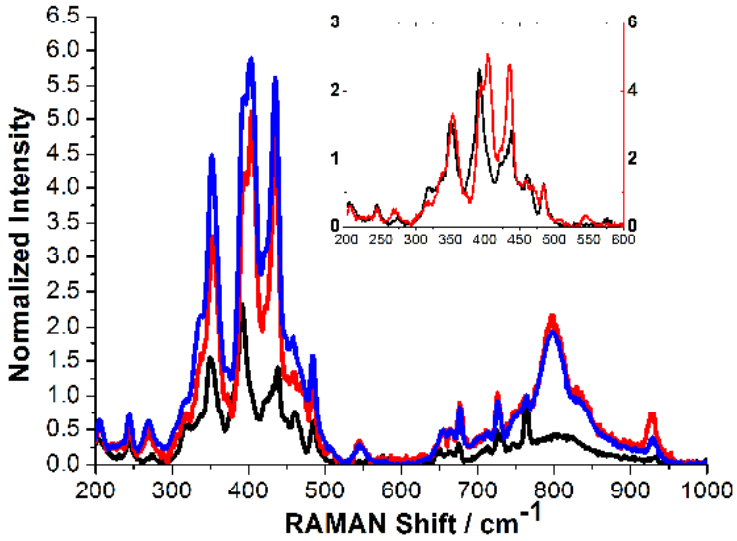

Figure 5. rRaman spectrums 30 s (red) and 2.73 h (blue) after the addition of 100 equivalents of CAN to a 1 mM solution of **1-dm**$^{4+}$ in 0.1 M HOTf at 25 °C. The spectrum before the reaction is also included (black). The inset shows en enlargement in the 200-600 cm^{-1} region.

4. Conclusions.

Mononuclear [TBRu^{II}-OH$_2$] complexes behave as water oxidation catalysts in the presence of a large excess of Ce(IV). In parallel this mononuclear complexes also suffer from ligand loss and formation of a dinuclear oxo-bridged complexes that are also active WOCs. As expected their high oxidation states are also highly active agents for the oxidation of organic substrates, producing a series of polynuclear complexes at reduced oxidation states and manifesting the existence of an oligomerization process.

We have isolated dinuclear, trinuclear and tetranuclear oxo-bridged complexes that have been structurally characterized by single crystal X-ray diffraction analysis. Their structural properties have been correlated to their electronic structure.

Finally the structural, electrochemical and reactivity properties of the oxo-bridged dimer **1-dm**$^{4+}$ has been thoroughly studied. In particular rR spectroscopy clearly shows that the catalytic oxidation of water to dioxygen observed is due to a reorganization of **1-dm**$^{4+}$ into **1-dn**$^{4+}$, after the addition after the addition of Ce(IV).

ASSOCIATED CONTENT

Supporting Information. Electronic supplementary information (ESI) available: Additional spectroscopic, electrochemical and reactivity experiments together with CIF files (CCDC # 1016623-1016632) and crystallographic information. This material is available free of charge via the Internet at http://pubs.acs.org.

AUTHOR INFORMATION

Corresponding Author

E-mail: allobet@iciq.cat.

Notes

The authors declare no competing financial interest.

ACKNOWLEDGMENT

Support from MINECO (CTQ-2013-49075-R, SEV-2013-0319 and PRI-PIBIN-2011-1278) is gratefully acknowledged. SM thanks MINECO for a Torres Quevedo contract and IL for a FPU grant.

REFERENCES

1. Bertini, I.; Lalli, D.; Mangani, S.; Pozzi, C.; Rosa, C.; Theil, E. C.; Turano, P. *J. Am. Chem. Soc.* **2012**, *134*, 6169.

2. Tshuva, E. Y.; Lippard, S. J. *Chem. Rev. (Washington, DC, U. S.)* **2004**, *104*, 987.

3. Vincent, J. B.; Olivier-Lilley, G. L.; Averill, B. A. *Chem. Rev. (Washington, DC, U. S.)* **1990**, *90*, 1447.

4. Sens, C.; Romero, I.; Rodríguez, M.; Llobet, A.; Parella, T.; Benet-Buchholz, J. *J. Am. Chem. Soc.* **2004**, *126*, 7798.

5. Zong, R.; Thummel, R. P. *J. Am. Chem. Soc.* **2005**, *127*, 12802.

6. Deng, Z.; Tseng, H.-W.; Zong, R.; Wang, D.; Thummel, R. *Inorg. Chem.* **2008**, *47*, 1835.

7. Xu, Y.; Åkermark, T. r.; Gyollai, V.; Zou, D.; Eriksson, L.; Duan, L.; Zhang, R.; Åkermark, B. r.; Sun, L. *Inorg. Chem.* **2009**, *48*, 2717.

8. Karlsson, E. A.; Lee, B.-L.; Åkermark, T.; Johnston, E. V.; Kärkäs, M. D.; Sun, J.; Hansson, Ö.; Bäckvall, J.-E.; Åkermark, B. *Angew. Chem. Int. Ed.* **2011**, *50*, 11715.

9. Sartorel, A.; MiroÌ , P.; Salvadori, E.; Romain, S.; Carraro, M.; Scorrano, G.; Valentin, M. D.; Llobet, A.; Bo, C.; Bonchio, M. *J. Am. Chem. Soc.* **2009**, *131*, 16051.

10. Geletii, Y. V.; Botar, B.; Kögerler, P.; Hillesheim, D. A.; Musaev, D. G.; Hill, C. L. *Angew. Chem. Int. Ed.* **2008**, *47*, 3896.

11. Yin, Q.; Tan, J. M.; Besson, C.; Geletii, Y. V.; Musaev, D. G.; Kuznetsov, A. E.; Luo, Z.; Hardcastle, K. I.; Hill, C. L. *Science* **2010**, *328*, 342.

12. Lv, H.; Geletii, Y. V.; Zhao, C.; Vickers, J. W.; Zhu, G.; Luo, Z.; Song, J.; Lian, T.; Musaev, D. G.; Hill, C. L. *Chem. Soc. Rev.* **2012**, *41*, 7572.

13. Concepcion, J. J.; Jurss, J. W.; Templeton, J. L.; Meyer, T. J. *J. Am. Chem. Soc.* **2008**, *130*, 16462.

14. Tseng, H.-W.; Zong, R.; Muckerman, J. T.; Thummel, R. *Inorg. Chem.* **2008**, *47*, 11763.

15. Concepcion, J. J.; Tsai, M.-K.; Muckerman, J. T.; Meyer, T. J. *J. Am. Chem. Soc.* **2010**, *132*, 1545.

16. Wasylenko, D. J.; Ganesamoorthy, C.; Henderson, M. A.; Koivisto, B. D.; Osthoff, H. D.; Berlinguette, C. P. *J. Am. Chem. Soc.* **2010**, *132*, 16094.

17. Polyansky, D. E.; Muckerman, J. T.; Rochford, J.; Zong, R.; Thummel, R. P.; Fujita, E. *J. Am. Chem. Soc.* **2011**, *133*, 14649.

18. Wasylenko, D. J.; Ganesamoorthy, C.; Koivisto, B. D.; Henderson, M. A.; Berlinguette, C. P. *Inorg. Chem.* **2010**, *49*, 2202.

19. López, I.; Ertem, M. Z.; Maji, S.; Benet-Buchholz, J.; Keidel, A.; Kuhlmann, U.; Hildebrandt, P.; Cramer, C. J.; Batista, V. S.; Llobet, A. *Angew. Chem. Int. Ed.* **2014**, *53*, 205.

20. *Activation of Small Molecules*; 1st ed.; Tolman, W. B., Ed.; WILEY-VCH: Weinheim, Germany, 2006.

21. Suzuki, M. *Acc. Chem. Res.* **2007**, *40*, 609.

22. Cramer, C. J.; Tolman, W. B. *Acc. Chem. Res.* **2007**, *40*, 601.

23. Takeuchi, K. J.; Thompson, M. S.; Pipes, D. W.; Meyer, T. J. *Inorg. Chem.* **1984**, *23*, 1845.

24. Maji, S.; López, I.; Bozoglian, F.; Benet-Buchholz, J.; Llobet, A. *Inorg. Chem.* **2013**, *52*, 3591.

25. v2009.1-0.2 ed.; Bruker AXS Inc.: Madison, Wisconsin, USA, 2009.

26. V7.60A ed.; Bruker AXS Inc.: Madison, Wisconsin, USA, 2007.

27. Sheldrick, G. *Acta Crystallographica Section A* **2008**, *64*, 112.

28. Spek, A. *J. Appl. Crystallogr.* **2003**, *36*, 7.

29. Zanella, A. W.; Ford, P. C. *Inorg. Chem.* **1975**, *14*, 42.

30. Mola, J.; Pujol, D.; Rodríguez, M.; Romero, I.; Sala, X.; Katz, N.; Parella, T.; Benet-Buchholz, J.; Fontrodona, X.; Llobet, A. *Aust. J. Chem.* **2009**, *62*, 1675.

31. Weaver, T. R.; Meyer, T. J.; Adeyemi, S. A.; Brown, G. M.; Eckberg, R. P.; Hatfield, W. E.; Johnson, E. C.; Murray, R. W.; Untereker, D. *J. Am. Chem. Soc.* **1975**, *97*, 3039.

32. Llobet, A.; Curry, M. E.; Evans, H. T.; Meyer, T. J. *Inorg. Chem.* **1989**, *28*, 3131.

33. Neubold, P.; Wieghardt, K.; Nuber, B.; Weiss, J. *Inorg. Chem.* **1989**, *28*, 459.

34. Dobson, J. C.; Sullivan, B. P.; Doppelt, P.; Meyer, T. J. *Inorg. Chem.* **1988**, *27*, 3863.

35. Schoonover, J. R.; Ni, J.; Roecker, L.; White, P. S.; Meyer, T. J. *Inorg. Chem.* **1996**, *35*, 5885.

36. Masuda, H.; Taga, T.; Osaki, K.; Sugimoto, H.; Mori, M.; Ogoshi, H. *Bull. Chem. Soc. Jpn.* **1982**, *55*, 3887.

37. Masuda, H.; Taga, T.; Osaki, K.; Sugimoto, H.; Mori, M.; Ogoshi, H. *J. Am. Chem. Soc.* **1981**, *103*, 2199.

38. Deloume, J. P.; Faure, R.; Thomas-David, G. *Acta Crystallogr., Sect. B: Struct. Sci.* **1979**, *35*, 558.

39. Che, C. M.; Tang, W. T.; Wong, W. T.; Lai, T. F. *J. Am. Chem. Soc.* **1989**, *111*, 9048.

40. Fletcher, J. M.; Greenfield, B. F.; Hardy, C. J.; Scargill, D.; Woodhead, J. L. *J. Chem. Soc.* **1961**, *0*, 2000.

41. Vernik, I.; Stynes, D. V. *Inorg. Chem.* **1998**, *37*, 10.

42. Barral, M. C.; Jimenez-Aparicio, R.; Royer, E. C.; Saucedo, M. J.; Urbanos, F. A.; Gutierrez-Puebla, E.; Ruiz-valero, C. *J. Chem. Soc., Dalton Trans.* **1991**, *0*, 1609.

43. Biswas, M. K.; Patra, S. C.; Maity, A. N.; Ke, S.-C.; Weyhermuller, T.; Ghosh, P. *Chem. Commun. (Cambridge, U. K.)* **2013**, *49*, 4522.

44. Carter, L.; Davies, D. L.; Fawcett, J.; Russell, D. R. *Polyhedron* **1993**, *12*, 1599.

45. Sahli, Z.; Derrien, N.; Pascal, S.; Demerseman, B.; Roisnel, T.; Barriere, F.; Achard, M.; Bruneau, C. *Dalton Trans.* **2011**, *40*, 5625.

46. Llobet, A.; Doppelt, P.; Meyer, T. J. *Inorg. Chem.* **1988**, *27*, 514.

47. Schneider, R.; Weyhermueller, T.; Wieghardt, K.; Nuber, B. *Inorg. Chem.* **1993**, *32*, 4925.

48. Liu, F.; Concepcion, J. J.; Jurss, J. W.; Cardolaccia, T.; Templeton, J. L.; Meyer, T. J. *Inorg. Chem.* **2008**, *47*, 1727.

49. Jurss, J. W.; Concepcion, J. J.; Butler, J. M.; Omberg, K. M.; Baraldo, L. M.; Thompson, D. G.; Lebeau, E. L.; Hornstein, B.; Schoonover, J. R.; Jude, H.; Thompson, J. D.; Dattelbaum, D. M.; Rocha, R. C.; Templeton, J. L.; Meyer, T. J. *Inorg. Chem.* **2012**, *51*, 1345.

50. Sanders-Loehr, J.; Wheeler, W. D.; Shiemke, A. K.; Averill, B. A.; Loehr, T. M. *J. Am. Chem. Soc.* **1989**, *111*, 8084.

51. Lebeau, E. L.; Adeyemi, S. A.; Meyer, T. J. *Inorg. Chem.* **1998**, *37*, 6476.

52. Ishitani, O.; White, P. S.; Meyer, T. J. *Inorg. Chem.* **1996**, *35*, 2167.

53. Gilbert, J. A.; Eggleston, D. S.; Murphy, W. R.; Geselowitz, D. A.; Gersten, S. W.; Hodgson, D. J.; Meyer, T. J. *J. Am. Chem. Soc.* **1985**, *107*, 3855.

54. Phelps, D. W.; Kahn, E. M.; Hodgson, D. J. *Inorg. Chem.* **1975**, *14*, 2486.

55. Earley, J. E.; Smith, P. M.; Fealey, T.; Silverton, J. V. *Inorg. Chem.* **1971**, *10*, 1943.

56. Schulz, L. D.; Fallon, G. D.; Moubaraki, B.; Murray, K. S.; West, B. O. *J. Chem. Soc., Chem. Commun.* **1992**, *0*, 971.

57. Francas, L.; Sala, X.; Escudero-Adan, E.; Benet-Buchholz, J.; Escriche, L.; Llobet, A. *Inorg. Chem.* **2011**, *50(7),* 2771-2781.

58. Sala, X.; Maji, S.; Bofill, R.; García-Antón, J.; Escriche, L.; Llobet, A. *Acc. Chem. Res*., **2014**, *47*(2), 504-516.

TOC

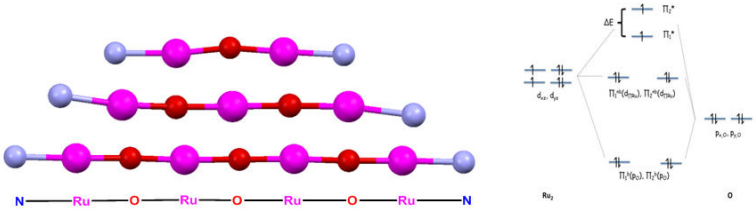

Synopsis: A variety of linear polynuclear oxo-bridged Ru complexes including dinuclear, trinuclear and tetranuclear Ru complexes have been obtained within the framework of the side reactions involved in the so-called single site water oxidation catalyst. These complexes have been structurally characterized by single crystal X-Ray diffraction analysis and the water oxidation activity of some of them is discussed.